Physics Letters B 774 (2017) 14–19

Contents lists available at ScienceDirect

Physics Letters B

www.elsevier.com/locate/physletb

Two-proton emission half-lives in the effective liquid drop model

M. Gonçalves [a,*], N. Teruya [b], O.A.P. Tavares [c], S.B. Duarte [c]

[a] Comissão Nacional de Energia Nuclear, R. Gal. Severiano, 22290-151, Rio de Janeiro, Brazil
[b] Universidade Federal da Paraíba — 58051-970 João Pessoa, Brazil
[c] Centro Brasileiro de Pesquisas Físicas — R. Dr. Xavier Sigaud 150, 22290-180, Rio de Janeiro, Brazil

ARTICLE INFO

Article history:
Received 4 March 2017
Received in revised form 26 July 2017
Accepted 13 September 2017
Available online 18 September 2017
Editor: J.-P. Blaizot

Keywords:
2p-emission
Proton-rich nuclei
Half-life estimate
Effective liquid drop model

ABSTRACT

Half-life for two-proton radioactivity of emitter nuclides of mass number $A < 70$ has been calculated by using a phenomenological, effective liquid drop model (ELDM) which has been applied successfully to one-proton radioactivity, alpha decay, cluster radioactivity and cold fission processes. Following this approach, we estimate half-life values for several 2p-emitted nuclides and compare our results with predictions from other models, as well as the existing data in the literature, specifically the cases for ^{16}Ne, ^{19}Mg, ^{45}Fe, ^{48}Ni, ^{54}Zn and ^{67}Kr parent nuclei. It is seen that the ELDM version adapted to deal with 2p-decay process reproduces the available experimental data quite satisfactorily, asserting that shell corrections and pairing effects for the ground state nucleus have been well incorporated into the model via the experimental mass excess values. The present estimates for half-lives show a number of nuclei with detectable 2p-emission mode, which predictions may serve as indicators for further experimental investigations.

1. Introduction

Two-proton (2p) radioactivity has been predicted since 1960 [1–3] and, due to the pairing energy, 2p-radioactivity candidates are not allowed to decay by a sequential emission of two protons, since the one-proton emission from the first daughter is not accessible energetically [4]. The 2p-radioactivity from ^{45}Fe was firstly observed in 2002 [5,6], and it is not clear up to now if this decay mode occurs as an uncorrelated simultaneous isotropic emission or as an emission of a strongly correlated pair of protons. In addition, experimental evidences point to the $A \approx 50$ mass region as being the most favorable for this new radioactive decay mode. Recently, the 2p-radioactivity from ^{54}Zn and ^{48}Ni isotopes has been observed [7,8].

A few years ago, an experiment performed at GANIL/LISE3 [7] showed for the first time eight events related to the existence of ^{54}Zn 2p-emitter. This nucleus, together with two other ones (^{45}Fe and ^{48}Ni), form a set of nuclei very near to the proton drip line, doubly or almost doubly magic nuclei, which may decay through the emission of a ^{2}He particle [8]. Other experimental results for ^{45}Fe and ^{48}Ni 2p-decay were additionally obtained as reported in [9], and 2p-radioactive decay from an abnormal spinning long-lived state of ^{94}Ag isotope was also reported for the first time by Mukha et al. [10]. Such a decay has been attributed by the authors to a large prolate deformation of the decaying nucleus, thus allowing the emission of protons throughout the pole regions (this case will not be treated here once we are applying a model suitable for nearly spherical nuclear configurations). Besides, a decade ago, the first direct, unambiguous identification of 2p-decay of ^{45}Fe was attained at GANIL [11]. Surprisingly, a novel result has appeared quite recently with the observation of 2p-radioactivity of ^{67}Kr, detected in an experiment conducted at RIKEN Nishina Center (Japan), in which it was measured a decay energy of 1.69 MeV and a partial half-life for 2p emission of (20 ± 7) ms [12].

From the theoretical point of view, during the last decades several approaches have been used to describe the emission mechanism and to determine typical half-life values for this decay mode. In 1991, Brown [13] considered the direct 2p-decay from nuclei of atomic number Z in the range 22–28 on the basis of a shell model with mass extrapolation. Properties of proton-rich nuclei at the sd-fp-shell boundary with A in the range 37–48 have been also investigated within the framework of the nuclear shell model by Ormand [14]. Self-consistent mean-field theories (Hartree–Fock, Hartree–Fock–Bogoliubov, and relativistic mean field theory) have been used by Nazarewicz et al. [15] to study a number of properties (2p-separation energy, deformation, single-particle level, proton average potential, 2p-partial decay half-life) of proton-rich nuclei around the double magic ^{48}Ni nucleus.

* Corresponding author.
E-mail address: mgoncalves@cnen.gov.br (M. Gonçalves).

http://dx.doi.org/10.1016/j.physletb.2017.09.032

Other important contributions are found in the literature. Cole [16] has investigated the decay properties of proton-rich nuclei with Z in the range 19–30 by using measured analog neutron-rich nuclei binding energies and Coulomb energy shifts deduced from a parametrization of measured Coulomb displacement energies. In addition, the width of the ^{12}O ground state due to ^{2}He emission was analyzed by Barker [17] by using the R-matrix formalism. Grigorenko et al. [18,19] investigated the dependence of half-life upon $2p$-decay energy for ^{45}Fe, ^{48}Ni, ^{54}Zn, ^{58}Ge, ^{62}Se, and ^{66}Kr in the framework of the three body model, *i.e.*, a nuclear core added of two protons. Recently, Olsen et al. [20] also applied their model to take into account updated nuclear density parameters to extend calculations to nuclei heavier than Strontium.

As it is seen, model scenarios are still not completely clear [21, 22], and the existing experimental data do not provide a definitive and unique model choice. Here, we applied a phenomenological model previously developed by us [23,24] to predict half-life values for nuclear $2p$-emission and comparing these values with other theoretical estimates and with existing data. The referred model, known as "effective liquid drop model" (ELDM), has given excellent results for one-proton and other exotic radioactive decay processes [25–28], as well as for very asymmetric spontaneous nuclear binary cold fragmentation [29,30].

2. Summary of the Effective Liquid Drop Model — ELDM

The basis for the ELDM consists in analytical calculations for the Coulomb and surface energies of the dinuclear shape parametrization, thus obtaining the barrier penetrability factor for a range of daughter and $2p$-system, with mass asymmetry covering all configurations with positive energy released (Q-value) (for a detailed description of the model see Refs. [23,29]). Shell effects have been effectively included in the model via the Q-value of the corresponding $2p$-emission process,

$$Q = \Delta M_{\mathcal{P}} - \left(\Delta M_{2p} + \Delta M_{\mathcal{D}}\right), \tag{1}$$

where $\Delta M_{\mathcal{P}}$, ΔM_{2p} and $\Delta M_{\mathcal{D}}$ denote the mass excesses for the parent, $2p$-system and daughter nuclei, respectively, taken from the Mass Table by Wang et al. [31,32] (since the $2p$-system — or ^{2}He — is an unbound system its mass excess is twice the proton excess mass, *i. e*, $\Delta M_{2p} = 2 \times \Delta M_p = 2 \times 7.289$ MeV $= 14.578$ MeV).

The emission process is characterized by a molecular-like phase, where the daughter nucleus and ^{2}He partners are overlapping (Fig. 1). Accordingly, the present ELDM considers explicitly the Coulomb and surface energy contributions to the potential barrier. For the first one, it has been made use of Gaudin's expression [33] for the electrostatic energy of two overlapping spherical segments with a uniform charge density,

$$V_c = \frac{8\pi}{9} a^5 \varepsilon(\theta_{2p}, \theta_{\mathcal{D}}) \rho_c, \tag{2}$$

where ρ_c is the initial charge density, $\varepsilon(\theta_{2p}, \theta_{\mathcal{D}})$ is a function of the angular variables, and a is the radius of the sharp neck (Fig. 1).

In this situation, a description for the effective mass transfer of the dinuclear system preserves the mass asymmetry of final fragments, namely, the *constant mass asymmetry shape* (CMAS — see Refs. [24–28]). Gamow's penetrability factor is calculated by considering two different inertia coefficients: the effective [24] and Werner–Wheeler's [34] ones.

At this point, we wish to emphasize the effective character of the potential barrier of the ELDM. During the molecular-like phase, the surface potential energy is introduced in terms of an effective surface tension, σ_{eff}, defined through the equation

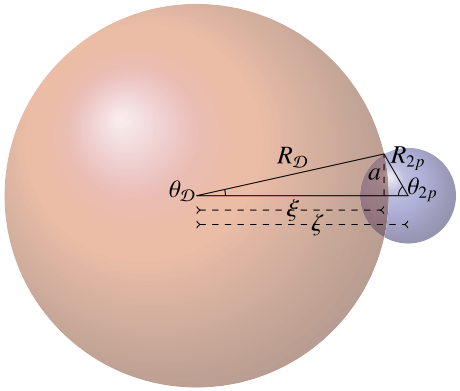

Fig. 1. Schematic representation of the molecular phase of the dinuclear system. The daughter nucleus and the emitted (smaller) fragments have radius $R_{\mathcal{D}}$ and R_{2p}, respectively, and the distance between their geometrical centers is denoted by ζ. The variable ξ represents the distance between the center of the heavier fragment and the circular sharp neck of radius a.

$$\frac{3}{5}e^2\left[\frac{Z_{\mathcal{P}}^2}{R_{\mathcal{P}}} - \frac{Z_{2p}^2}{\bar{R}_{2p}} - \frac{Z_{\mathcal{D}}^2}{\bar{R}_{\mathcal{D}}}\right] + 4\pi\sigma_{\text{eff}}\left(R_{\mathcal{P}}^2 - \bar{R}_{2p}^2 - \bar{R}_{\mathcal{D}}^2\right) = Q, \tag{3}$$

where $Z_i e$ ($i = \mathcal{P}$, $2p$, $\mathcal{D}$) are the nuclear charges, respectively, for the parent, emitted, and daughter nuclei. The final radii of the fragments are evaluated as

$$\bar{R}_i = \left(\frac{Z_i}{Z_{\mathcal{P}}}\right)^{1/3} R_{\mathcal{P}} \qquad (i = 2p, \mathcal{D}), \tag{4}$$

to be consistent with the uniform charge distribution considered in the Coulomb potential. The radius of the parent nucleus is assumed to be

$$R_{\mathcal{P}} = r_0 A_{\mathcal{P}}^{1/3}, \tag{5}$$

where r_0 is a free parameter of the model. We remark that the definition for the surface tension (Eq. (3)) establishes the effective character of the ELDM, since the energy difference between the initial and final configurations of the system reproduces correctly the energy released in the disintegration, *i.e.*, the Q-value. Therefore, the surface potential energy reads

$$V_s = \sigma_{\text{eff}}(S_{2p} + S_{\mathcal{D}}), \tag{6}$$

where S_{2p} and $S_{\mathcal{D}}$ denote the area of the surfaces for the emitted and daughter nuclei, respectively, and they are obtained as

$$S_{2p} = 2\pi R_{2p}(R_{2p} + \zeta - \xi) \qquad \text{and}$$
$$S_{\mathcal{D}} = 2\pi R_{\mathcal{D}}(R_{\mathcal{D}} + \xi). \tag{7}$$

Although the ELDM has been developed under the assumption of spherical fragments, the effect of fragment deformation is partially taken into account in the height of the barrier through the Q-value of the reaction. The effective separation of fragments at contact is dictated by the nuclear radius parameter, r_0. Some examples of the potential barrier following the ELDM applied to $2p$-emission from nuclei are shown in Fig. 2. There, the surface and Coulomb components of the potential barrier, as well as the total potential barrier, are depicted for ^{19}Mg, ^{45}Fe and ^{67}Kr. These examples cover a wide range of $2p$-emitter nuclei. In the figure we note that for more massive nuclei, the Coulomb barrier gains significant importance over the nuclear barrier (parts (b) and (c) in Fig. 2). This Coulomb barrier height will be determinant on $2p$-emission half-life, since it affects directly Gamow's penetrability factor. On the other hand, one observes a steeper and thicker barrier for heavier parent nuclei. In general, we can state that the

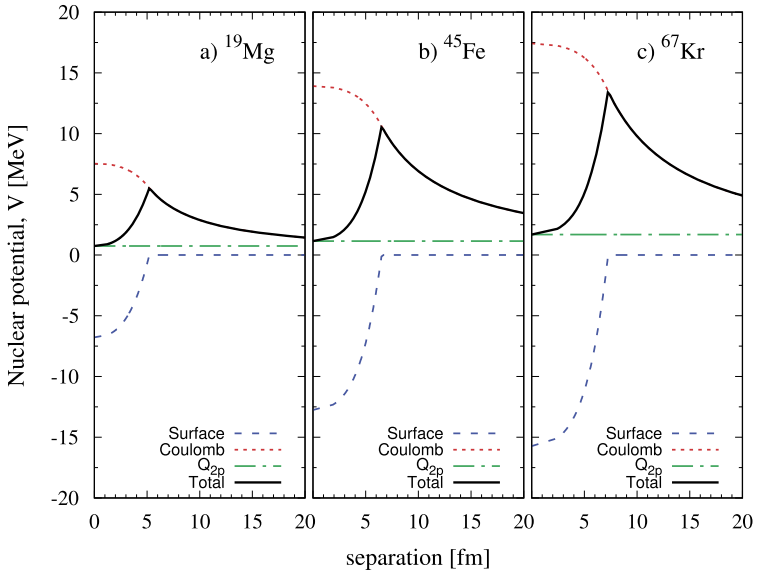

Fig. 2. Coulomb, surface, and total potential energy as a function of separation between centers of fragments, ζ, for $2p$-decay of ^{19}Mg, ^{45}Fe and ^{67}Kr following the ELDM model.

Coulomb barrier is responsible to at least 60% of the total area (Gamow's penetrability), this percentage increasing strongly with the charge of the decaying nucleus.

It may happen that in a nuclear $2p$-emission the spin-parity of the parent nucleus differs from that of the daughter nucleus. In these cases, the spin and parity conservation laws lead to an angular momentum $\ell \neq 0$. The effect of this centrifugal potential energy,

$$V_\ell = \frac{\ell(\ell+1)\hbar^2}{2\mu\zeta^2}, \tag{8}$$

contributes to the total potential barrier (here, μ represents the reduced mass of the $2p$-disintegration system). Therefore, for all these cases, the effective, total potential energy is constructed as

$$V = V_c + V_s + V_\ell. \tag{9}$$

The quantum transition rate from the initial to final state of the system has been determined by reducing the problem to an one-dimensional motion, the emitted fragments separation, ζ, in Gamow's theory. The penetrability factor, G, is calculated under the assumption that the system tunnels a barrier of height $V - Q$. Shell effects, which appear in the Q-value, act directly on the height and width of the effective barrier. Accordingly,

$$G = \exp\left\{-\frac{2}{\hbar}\int_{\zeta_0}^{\zeta_c}\sqrt{2\mu[V(\zeta)-Q]}d\zeta\right\}. \tag{10}$$

The limits of integration are the inner turning point, $\zeta_0 = R_{\mathcal{P}} - \bar{R}_{2p}$, and the outer turning point which is, for null angular momentum, given by $\zeta_c = Z_{2p}Z_{\mathcal{D}}e^2/Q$. Finally, the half-life is calculated as $\tau = \frac{\ln 2}{\lambda}$, where $\lambda = \lambda_0 G$, in which λ_0 is related to the frequency of assaults to the barrier and the preformation probability rate of the strongly correlated $2p$ at the surface of the emitter nucleus (see, for instance, Ref. [29]). A typical value for λ_0 is in the range 10^{19}–10^{21} assaults per second, and we have used $\lambda_0 = 4.96 \times 10^{19}$ throughout the present calculation.

3. Estimates of $2p$ emission half-life with ELDM

Calculations have been performed in order to reproduce the reliable $2p$-decay half-life for the case $^{45}\text{Fe} \rightarrow {}^{43}\text{Cr}$ by only varying the value of parameter r_0 of the ELDM (Eq. (5)). Among the four descriptions proposed to describe nuclear spontaneous processes from proton-radioactivity to cold fission (see Ref. [29]), the cluster-like approach with Werner–Wheeler's inertial coefficient revealed as the most suitable in dealing with $2p$-emission from intermediate-mass nuclei, since the preformation characteristics of the $2p$-system conforms better with the basic idea of an existing cluster defined within the parent nuclei environment. Thus, we focus our attention to results from this above mentioned approach, *i.e.*, the constant mass asymmetry description with Werner–Wheeler's inertial coefficient, referred to as WW-CMAS.

We have used the well-known $2p$-decay from ^{45}Fe nucleus to fix r_0 value. The best result which reaches the average experimental half-life value for this decay ($\langle\tau_{\text{exp}}\rangle = 3.6$ ms) [see Table 1] was found $r_0 = 1.12$ fm. This value was the one used throughout the entire investigation in the present work. Therefore, according to assumption defined in Eqs. (4) and (5) the radius of the emitted $2p$ (or ^{2}He) results proportional to $\sqrt[3]{\frac{A_P}{Z_P}}$, thus varying in the interval 1.65–1.74 fm for parent nuclei in the mass range $16 \leq A_P \leq 67$ (a variation of 5% only).

In order to examine the differences among the estimates from various models regarding calculated $2p$-emission half-lives and the experimental data, Table 1 summarizes such results. Half-life-values of the present study have been obtained with the WW-CMAS approach of the ELDM. By comparing calculated and measured half-life values for six parent nuclei (^{16}Ne, ^{19}Mg, ^{45}Fe, ^{48}Ni, ^{54}Zn and ^{67}Kr), as listed in Table 1, one observes that the results obtained via the WW-CMAS approach agree quite well with measured values. A large discrepancy, however, is seen in the case for ^{16}Ne, since the theoretical half-life value deviates by nearly four orders of magnitude from the measured value. We suspect that, since the half-life for ^{16}Ne was measured so small as $\approx 10^{-21}$ s, the experimental uncertainty in this process could be very large, magnifying the range of detectable $2p$ emission from the parent ^{16}Ne nucleus. From the theoretical point of view, we do not expect that deformation or collective mechanisms could affect so severely our half-life

Table 1
Comparison between experimental and calculated half-life-values for nuclear decay by $2p$-emission from ^{16}Ne, ^{19}Mg, ^{45}Fe, ^{48}Ni, ^{54}Zn and ^{67}Kr nuclei.

Decay case	Experimental			Calculated		
	Q_{2p} [MeV]	Half-life τ_e [ms]	Ref.	Q_{2p} [MeV]	Half-life τ_c [ms]	Ref.
$^{16}\text{Ne} \rightarrow {}^{14}\text{O}$	1.33	2.3×10^{-18}	[35]	1.401[a]	**2.54** $\times 10^{-14}$	this work
	1.4	4.2×10^{-18}	[36]			
$^{19}\text{Mg} \rightarrow {}^{17}\text{Ne}$	–	$(4 \pm 1.5)\times10^{-9}$	[20]	0.75[a]	**1.89** $\times 10^{-9}$	this work
	0.75 ± 0.05	$(6^{+2}_{-4})\times10^{-9}$	[37]			
$^{45}\text{Fe} \rightarrow {}^{43}\text{Cr}$	–	3.7 ± 0.4	[20]	1.279 ± 0.181	10^{-5}–10^{-1}	[14]
	1.21 ± 0.05	3.76 ± 0.26	[38]	1.154 ± 0.094	2×10^{-3}–0.3	[13]
	1.15	3.7 ± 0.3	[39]	1.154[a]	**3.70**	this work
	1.15	$3.5^{+1.6}_{-0.8}$	[11]			
	1.14 ± 0.04	$4.7^{+3.4}_{-1.4}$	[5]			
	1.1 ± 0.1	$4^{+2}_{-1.3}$	[6]			
	1.154 ± 0.016	$3^{+0.8}_{-0.6}$	[9]			
	1.15	$2.3^{+1.3}_{-0.6}$	[4]			
	–	$3.6^{+1.4}_{-0.7}$ [(b)]	–			
$^{48}\text{Ni} \rightarrow {}^{46}\text{Fe}$	1.35 ± 0.02	$8.4^{+12.8}_{-7}$	[9]	1.357 ± 0.130	10^{-3}–0.2	[39]
	1.29 ± 0.04	$3^{+2.2}_{-1.2}$	[21]	1.137 ± 0.210	10^{-2}–3.7×10^{3}	[14]
				1.290–1.357	0.3–75	[19]
				1.305[a]	**4.38**	this work
$^{54}\text{Zn} \rightarrow {}^{52}\text{Ni}$	1.48 ± 0.02	3.7^{+2}_{-1}	[7]	1.794 ± 0.46	–	[16]
	–	$1.98^{+0.73}_{-0.41}$	[20]	1.33 ± 0.14	–	[40]
	1.28 ± 0.21	$1.73^{+0.71}_{-0.47}$	[41]	1.33–1.873	5×10^{-7}–3.5	[19]
				1.48[a]	**3.03**	this work
$^{67}\text{Kr} \rightarrow {}^{65}\text{Se}$	1.690 ± 0.017	20 ± 8	[12]	1.538	> 15	[19]
				1.76 ± 0.14	0.046–4	[19,40]
				1.69[c]	**8.73** $\times 10^{2}$	this work
				1.577[d]	**1.09** $\times 10^{4}$	this work

[a] Taken from the AME 2016 Mass Table by Wang et al. [31,32].
[b] Average value.
[c] Measured value.
[d] Mean value from mass-excess-values following the droplet model of atomic nuclei proposed by Möller et al. [42].

prediction. Clearly, further investigation should take place concerning this issue. Considering the results reported in Table 1 we can say that the ELDM as previously summarized works as a simple and practical tool in evaluating half-life values of $2p$-radioactive process for a number of nuclei along the nuclide chart for which processes the Q_{2p}-value of the reaction is well known and a positive quantity. In addition, we remark that such calculations can also help in a discussion concerning the $2p$-decaying mode as a competing decay process, as it has been point out in recent investigations of $2p$-emission from ^{12}O isotope [17,43,44].

Thus, we extended our calculations to include $2p$ parent emitter nuclei of $Q_{2p} > 0$ listed in the 2016 Atomic Mass Evaluation by Wang et al. [31,32] in order to give a new insight on the half-life for this nuclear decay mode. This most recent, updated Mass Table [31,32] reports a total of fifty-nine cases of positive Q_{2p}-value of which forty cases of $\ell = 0$, sixteen of $\ell \neq 0$, and other three cases of undefined ℓ-values. The $2p$-emitter nuclides of $Q_{2p} > 0$ are seen concentrated into two ranges of Z (or A), namely, $3 \leq Z \leq 34$ ($3 \leq A \leq 64$, forty-one cases) and $68 \leq Z \leq 84$ ($142 \leq A \leq 186$, eighteen cases). There are not cases of Q_{2p} in the 2016 AME [31, 32] for parent nuclei of $34 < Z < 68$ ($64 < A < 142$) or $Z > 84$ ($A > 186$). For roughly half of these cases exhibiting $Q_{2p} > 1$ MeV, calculated half-life values have been obtained by making use of the ELDM for parent nuclei with $4 \leq Z \leq 33$ and ^{67}Kr (this latter, clearly not quoted in Ref. [31,32]). In Fig. 3, the ratio $q = Q_{2p}/V_c$ (total available energy for $2p$-decay to barrier height) has been chosen to represent the calculated half-life results of Table 2 and the experimental data.

Since calculations depend upon the Q_{2p}-value, results should be strongly sensitive to new and updated mass-values. In this aspect, the present model suggests that, due to the small mass of the $2p$-system, the mass transfer mechanism is unimportant in dealing with the preformed $2p$-system during the separation phase, even for cases of $2p$-radioactivity of lighter nuclei such as ^{12}O and ^{16}Ne. For the sake of completeness, calculations have been also performed by using the other three variants of the ELDM, namely, CMAS with other proposal for the inertia coefficient, and varying mass asymmetry (VMAS) with Werner–Wheeler or our inertia coefficients [23,29]. One certifies that results are roughly insensitive to the choice of the ELDM-approach, since a suitable definition of parameter r_0 could be taken into account to conform results to data.

4. Final remarks and conclusions

Present letter reports results from the extension of the phenomenological ELDM to the case of $2p$-emission, exploring the predictive power of the model in order to point out new promissory cases to be measured. The existing detected cases are repro-

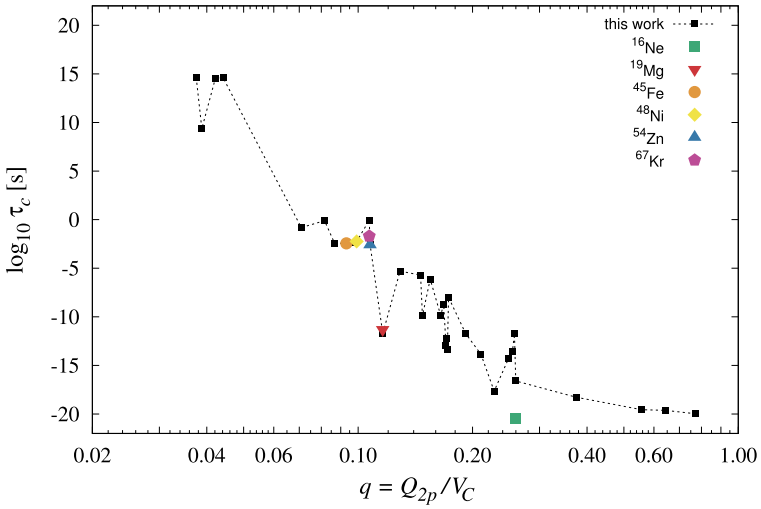

Fig. 3. Dependence of $2p$-decay half-life, τ, upon the ratio $q = Q_{2p}/V_c$ (V_c is the barrier height). Data points are those listed in Tables 1 (measured values) and 2 (calculated ones).

Table 2
Calculated $2p$-decay half-life, τ_c, for parent nuclei of $Q_{2p} > 0$ as quoted in the 2016 Mass Table by Wang et al. [31,32]. The WW-CMAS of ELDM with $\lambda_0 = 4.96 \times 10^{19}$ s^{-1} and $r_0 = 1.12$ fm have been used in all cases.

Decay case ($2p$-emission)	ℓ[a,b]	Q_{2p} [MeV]	Half-life τ_c [s]	Decay case ($2p$-emission)	ℓ[a,b]	Q_{2p} [MeV]	Half-life τ_c [s]
^{6}Be $\rightarrow$ ^{4}He $+2p$	0	1.372	1.08×10^{-20}	^{42}Cr $\rightarrow$ ^{40}Ti $+2p$	0	1.002	3.73×10^{-3}
^{7}B $\rightarrow$ ^{5}Li $+2p$	0	1.42	2.80×10^{-20}	^{45}Fe $\rightarrow$ ^{43}Cr $+2p$	0	1.154	3.70×10^{-3}
^{8}C $\rightarrow$ ^{6}Be $+2p$	0	2.111	2.38×10^{-20}	^{47}Co $\rightarrow$ ^{45}Mn $+2p$	0	1.042	7.86×10^{-1}
^{10}N $\rightarrow$ ^{8}B $+2p$	1	1.3	2.27×10^{-18}	^{48}Ni $\rightarrow$ ^{46}Fe $+2p$	0	1.305	4.38×10^{-3}
^{12}O $\rightarrow$ ^{10}C $+2p$	0	1.638	5.42×10^{-19}	^{49}Ni $\rightarrow$ ^{47}Fe $+2p$	0	0.492	4.38×10^{14}
^{16}Ne $\rightarrow$ ^{14}O $+2p$	0	1.401	2.54×10^{-17}	^{52}Cu $\rightarrow$ ^{50}Co $+2p$	4	0.772	2.30×10^{9}
^{19}Mg $\rightarrow$ ^{17}Ne $+2p$	0	0.75	1.89×10^{-12}	^{54}Zn $\rightarrow$ ^{52}Ni $+2p$	0	1.48	3.03×10^{-3}
^{22}Si $\rightarrow$ ^{20}Mg $+2p$	0	1.283	4.81×10^{-14}	^{56}Ga $\rightarrow$ ^{54}Cu $+2p$	0	2.443	1.01×10^{-8}
^{26}S $\rightarrow$ ^{24}Si $+2p$	0	1.755	1.39×10^{-14}	^{57}Ga $\rightarrow$ ^{55}Cu $+2p$	2	2.047	5.01×10^{-6}
^{28}Cl $\rightarrow$ ^{26}P $+2p$	2	1.965	1.13×10^{-13}	^{58}Ge $\rightarrow$ ^{56}Zn $+2p$	0	3.732	1.83×10^{-12}
^{30}Ar $\rightarrow$ ^{28}S $+2p$	0	2.28	4.82×10^{-15}	^{59}Ge $\rightarrow$ ^{57}Zn $+2p$	0	2.102	1.96×10^{-6}
^{32}K $\rightarrow$ ^{30}Cl $+2p$	2	2.077	5.65×10^{-13}	^{60}Ge $\rightarrow$ ^{58}Zn $+2p$	0	0.631	4.14×10^{14}
^{34}Ca $\rightarrow$ ^{32}Ar $+2p$	0	1.474	1.23×10^{-10}	^{60}As $\rightarrow$ ^{58}Ga $+2p$	4	3.492	2.08×10^{-9}
^{36}Sc $\rightarrow$ ^{34}K $+2p$	0	1.993	1.84×10^{-12}	^{61}As $\rightarrow$ ^{59}Ga $+2p$	0	2.282	7.61×10^{-7}
^{38}Ti $\rightarrow$ ^{36}Ca $+2p$	0	2.743	2.73×10^{-14}	^{62}As $\rightarrow$ ^{60}Ga $+2p$	2	0.692	3.30×10^{14}
^{39}Ti $\rightarrow$ ^{37}Ca $+2p$	0	0.758	1.54×10^{-1}	^{67}Kr $\rightarrow$ ^{65}Se $+2p$	0	1.69[c]	8.73×10^{-1}
^{40}V $\rightarrow$ ^{38}Sc $+2p$	0	1.842	1.40×10^{-10}				

[a] Nuclear spin and parity are taken from [45].
[b] Lowest angular momentum when different ℓ-values are possible.
[c] Measured value in Ref. [12].

duced with a quite satisfactory accuracy (except for ^{16}Ne), taking into account that the experimental results cover numerical values obtained for fifteen orders of magnitude in the half-life. This is shown in Fig. 3 and listed in Table 2, comparing our result with other models. Since our calculations strongly depend upon the Q_{2p}-value, we have used updated mass-values.

Finally, the work hypothesis of the calculation which consists in assuming the $2p$-system as a preformed system in the nuclear medium deserves some considerations. For sure, as soon the $2p$-system is outside the daughter nucleus the system dissociates and the two protons are separated by the dominance of the Coulomb repulsion. The preformation can be understood in the context of the macroscopic nature of the ELDM calling attention to other aspect concerning the tunneling process, where we remark that since the Q_p-value of one-proton emission is negative for the considered parent nuclei, there should be a flux of reflected protons at the surface barrier. Thus, one of the reflected protons can be combined together with another proton to form a pair due to the pairing correlation, not included in the mean field surface barrier. In addition, the pairing of the protons will contribute to minimize the local asymmetry energy in the region near and inside neutron skin. Here we are only trying to offer some arguments in favor of the plausibility of the model hypothesis. A deeper discussion on the $2p$-preformation involves microscopic structural aspects which are out of the scope of the model here presented.

Acknowledgements

This work has been partially supported by the Brazilian CNPq. The authors would like to thank to Dr. A.J. Dimarco for valuable discussions and suggestions at the beginning of this work.

References

[1] V. Goldansky, On neutron-deficient isotopes of light nuclei and the phenomena of proton and two-proton radioactivity, Nucl. Phys. 19 (1960) 482–495.

[2] V.I. Goldansky, About exotic nuclei having isospin T → A/2 and radiative capture of pions, Pisma Zh. Èksp. Teor. Fiz. 23 (1976) 366–368.

[3] F. Guzmán, M. Gonçalves, O.A.P. Tavares, S.B. Duarte, F. García, O. Rodríguez, Proton radioactivity from proton-rich nuclei, Phys. Rev. C 59 (1999) R2339–R2342.

[4] J. Giovinazzo, The two-proton radioactivity in the A approx. 50 mass region, J. Phys. G 31 (2005) S1509–S1515.

[5] J. Giovinazzo, B. Blank, M. Chartier, S. Czajkowski, A. Fleury, M.J. Lopez Jimenez, M.S. Pravikoff, J.C. Thomas, F. de Oliveira Santos, M. Lewitowicz, V. Maslov, M. Stanoiu, R. Grzywacz, M. Pfützner, C. Borcea, B.A. Brown, Two-proton radioactivity of F-45e, Phys. Rev. Lett. 89 (2002) 102501.

[6] M. Pfützner, E. Badura, C. Bingham, B. Blank, M. Chartier, H. Geissel, J. Giovinazzo, L.V. Grigorenko, R. Grzywacz, M. Hellström, Z. Janas, J. Kurcewicz, A.S. Lalleman, C. Mazzocchi, I. Mukha, G. Münzenberg, C. Plettner, E. Roeckl, K.P. Rykaczewski, K. Schmidt, R.S. Simon, M. Stanoiu, J.-C. Thomas, First evidence for two-proton decay of Fe-45, Eur. Phys. J. A 14 (2002) 279.

[7] B. Blank, A. Bey, G. Canchel, C. Dossat, A. Fleury, J. Giovinazzo, I. Matea, N. Adimi, F. De Oliveira, I. Stefan, G. Georgiev, S. Grévy, J.C. Thomas, C. Borcea, D. Cortina, M. Caamano, M. Stanoiu, F. Aksouh, B.A. Brown, F.C. Barker, W.A. Richter, First observation of 54Zn and its decay by two-proton emission, Phys. Rev. Lett. 94 (2005) 232501.

[8] B. Blank, M. Chartier, S. Czajkowski, J. Giovinazzo, M.S. Pravikoff, J.C. Thomas, G. de France, F. de Oliveira Santos, M. Lewitowicz, C. Borcea, R. Grzywacz, Z. Janas, M. Pfützner, On the discovery of doubly-magic ^{48}Ni, Phys. Rev. Lett. 84 (2000) 1116–1119.

[9] C. Dossat, A. Bey, B. Blank, A. Fleury, J. Giovinazzo, I. Matea, F. de Oliveira Santos, G. Georgiev, S. Grévy, I. Stefan, J.C. Thomas, N. Adimi, C. Borcea, D. Cortina Gil, M. Caamano, M. Stanoiu, F. Aksouh, B.A. Brown, L.V. Grigorenko, Two-proton radioactivity studies with Fe-45 and Ni-48, Phys. Rev. C 72 (2005) 054315.

[10] I. Mukha, E. Roeckl, L. Batist, A. Blazhev, J. Döring, H. Grawe, L. Grigorenko, M. Huyse, Z. Janas, R. Kirchner, M. La Cammara, C. Mazzocchi, S.L. Tabor, P. Van Duppen, Proton–proton correlations observed in two-proton radioactivity of 94Ag, Nature 439 (2006) 298–302.

[11] J. Giovinazzo, B. Blank, C. Borcea, G. Canchel, C. Demonchy, F. de Oliveira Santos, C. Dossat, S. Grevy, L. Hay, J. Huikari, S. Leblanc, I. Matea, J.-L. Pedroza, L. Perrot, J. Pibernat, L. Serani, C. Stodel, J.-C. Thomas, First direct observation of two protons in the decay of ^{45}Fe with a TPC, Phys. Rev. Lett. 99 (2007) 102501.

[12] T. Goigoux, P. Ascher, B. Blank, M. Gerbaux, J. Giovinazzo, S. Grévy, T. Kurtukian Nieto, C. Magron, P. Doornenbal, G.G. Kiss, S. Nishimura, P.-A. Söderström, V.H. Phong, J. Wu, D.S. Ahn, N. Fukuda, N. Inabe, T. Kubo, S. Kubono, H. Sakurai, Y. Shimizu, T. Sumikama, H. Suzuki, H. Takeda, J. Agramunt, A. Algora, V. Guadilla, A. Montaner-Piza, A.I. Morales, S.E.A. Orrigo, B. Rubio, Y. Fujita, M. Tanaka, W. Gelletly, P. Aguilera, F. Molina, F. Diel, D. Lubos, G. de Angelis, D. Napoli, C. Borcea, A. Boso, R.B. Cakirli, E. Ganioglu, J. Chiba, D. Nishimura, H. Oikawa, Y. Takei, S. Yagi, K. Wimmer, G. de France, S. Go, B.A. Brown, Two-proton radioactivity of ^{67}Kr, Phys. Rev. Lett. 117 (2016) 162501.

[13] B.A. Brown, Diproton decay of nuclei on the proton drip line, Phys. Rev. C 43 (1991) R1513–R1517, See also erratum: Phys. Rev. C 44 (1991) 924.

[14] W.E. Ormand, Properties of proton drip-line nuclei at the sd-fp-shell interface, Phys. Rev. C 53 (1996) 214–221.

[15] W. Nazarewicz, J. Dobaczewski, T.R. Werner, J.A. Maruhn, P.G. Reinhard, K. Rutz, C.R. Chinn, A.S. Umar, M.R. Strayer, Structure of proton drip-line nuclei around doubly magic 48Ni, Phys. Rev. C 53 (1996) 740–751.

[16] B.J. Cole, Stability of proton-rich nuclei in the upper sd shell and lower pf shell, Phys. Rev. C 54 (1996) 1240–1248.

[17] F.C. Barker, O-12 ground state decay by He-2 emission, Phys. Rev. C 63 (2001) 047303.

[18] L.V. Grigorenko, R.C. Johnson, I.G. Mukha, I.J. Thompson, M.V. Zhukov, Two-proton radioactivity and three-body decay: general problems and theoretical approach, Phys. Rev. C 64 (2001) 054002.

[19] L.V. Grigorenko, M.V. Zhukov, Two proton radioactivity and three body decay. 2. Exploratory studies of lifetimes and correlations, Phys. Rev. C 68 (2003) 054005.

[20] E. Olsen, M. Pfützner, N. Birge, M. Brown, W. Nazarewicz, A. Perhac, Landscape of two-proton radioactivity, Phys. Rev. Lett. 110 (2013) 222501, Erratum: Phys. Rev. Lett. 111 (2013) 139903.

[21] M. Pomorski, et al., Proton spectroscopy of Ni48, Fe46 and Cr44, Phys. Rev. C 90 (2014) 014311.

[22] Y. Ma, D. Fang, X. Sun, P. Zhou, Y. Togano, N. Aoi, H. Baba, X. Cai, X. Cao, J. Chen, Y. Fu, W. Guo, Y. Hara, T. Honda, Z. Hu, K. Ieki, Y. Ishibashi, Y. Ito, N. Iwasa, S. Kanno, T. Kawabata, H. Kimura, Y. Kondo, K. Kurita, M. Kurokawa, T. Moriguchi, H. Murakami, H. Ooishi, K. Okada, S. Ota, A. Ozawa, H. Sakurai, S. Shimoura, R. Shioda, E. Takeshita, S. Takeuchi, W. Tian, H. Wang, J. Wang, M. Wang, K. Yamada, Y. Yamada, Y. Yasuda, K. Yoneda, G. Zhang, T. Motobayashi, Different mechanism of two-proton emission from proton-rich nuclei 23Al and 22Mg, Phys. Lett. B 743 (2015) 306–309.

[23] M.G. Gonçalves, S.B. Duarte, Effective liquid drop description for the exotic decay of nuclei, Phys. Rev. C 48 (1993) 2409–2414.

[24] S.B. Duarte, M.G. Gonçalves, Effective inertial coefficient for the dinuclear regime of the exotic decay of nuclei, Phys. Rev. C 53 (1996) 2309–2312.

[25] S.B. Duarte, M.G. Gonçalves, O.A.P. Tavares, Importance of the inner potential barrier in nuclear spontaneous cold fission processes, Phys. Rev. C 56 (1997) 3414–3416.

[26] S.B. Duarte, O. Rodríguez, O.A.P. Tavares, M. Gonçalves, F. García, F. Guzmán, Cold fission description with constant and varying mass asymmetries, Phys. Rev. C 57 (1998) 2516–2522.

[27] O.A.P. Tavares, S.B. Duarte, O. Rodríguez, F. Guzmán, M. Gonçalves, F. García, Effective liquid drop description for alpha decay of atomic nuclei, J. Phys. G 24 (1998) 1757–1776.

[28] O. Rodríguez, F. Guzmán, S.B. Duarte, O.A.P. Tavares, F. García, M. Gonçalves, New valleys of cold fission and cluster radioactivity processes from nuclei far from the beta-stability line, Phys. Rev. C 59 (1999) 253–260.

[29] S.B. Duarte, O.A.P. Tavares, F. Guzmán, A. Dimarco, F. García, O. Rodríguez, M. Gonçalves, Half-lives for proton emission, alpha decay, cluster radioactivity, and cold fission processes calculated in a unified theoretical framework, At. Data Nucl. Data Tables 80 (2002) 235–299.

[30] S.B. Duarte, O.A.P. Tavares, M. Gonçalves, O. Rodríguez, F. Guzmán, T.N. Barbosa, F. García, A. Dimarco, Half-life predictions for decay modes of superheavy nuclei, J. Phys. G, Nucl. Part. Phys. 30 (2004) 1487–1494.

[31] W. Huang, G. Audi, M. Wang, F. Kondev, S. Naimi, X. Xu, The AME2016 atomic mass evaluation (I). Evaluation of input data, Chin. Phys. C 41 (2017) 030002.

[32] M. Wang, G. Audi, F. Kondev, W. Huang, S. Naimi, X. Xu, The AME2016 atomic mass evaluation (II). Tables, graphs and references, Chin. Phys. C 41 (2017) 030003.

[33] M. Gaudin, Énergie coulombienne du solide uniformément chargé limité par deux sphères sécantes, J. Phys. 35 (1974) 885–894.

[34] D.N. Poenaru, J.A. Maruhn, W. Greiner, M. Ivaşcu, D. Mazilu, I. Ivaşcu, Inertia and fission paths in a wide range of mass asymmetry, Z. Phys. A, At. Nucl. 333 (1989) 291–298.

[35] G.J. KeKelis, M.S. Zisman, D.K. Scott, R. Jahn, D.J. Vieira, J. Cerny, F. Ajzenberg-Selove, Masses of the unbound nuclei ^{16}Ne, ^{15}F, and ^{12}O, Phys. Rev. C 17 (1978) 1929–1938.

[36] C.J. Woodward, R.E. Tribble, D.M. Tanner, Mass of ^{16}Ne, Phys. Rev. C 27 (1983) 27–30.

[37] I. Mukha, Experimental studies of nuclei beyond the proton drip line by tracking technique, Eur. Phys. J. A 42 (2009) 421.

[38] L. Audirac, P. Ascher, B. Blank, C. Borcea, B.A. Brown, G. Canchel, C.E. Demonchy, F. de Oliveira Santos, C. Dossat, J. Giovinazzo, S. Grévy, L. Hay, J. Huikari, S. Leblanc, I. Matea, J.-L. Pedroza, L. Perrot, J. Pibernat, L. Serani, C. Stodel, J.-C. Thomas, Direct and β-delayed multi-proton emission from atomic nuclei with a time projection chamber: the cases of ^{43}Cr, ^{45}Fe and ^{51}Ni, Eur. Phys. J. A 48 (2012) 179.

[39] K. Miernik, W. Dominik, Z. Janas, M. Pfützner, L. Grigorenko, C.R. Bingham, H. Czyrkowski, M. Cwiok, I.G. Darby, R. Dabrowski, T. Ginter, R. Grzywacz, M. Karny, A. Korgul, W. Kuśmierz, S.N. Liddick, M. Rajabali, K. Rykaczewski, A. Stolz, Two-proton correlations in the decay of ^{45}Fe, Phys. Rev. Lett. 99 (2007) 192501.

[40] B.A. Brown, R.R.C. Clement, H. Schatz, A. Volya, W.A. Richter, Proton drip-line calculations and the rp process, Phys. Rev. C 65 (2002) 045802.

[41] P. Ascher, L. Audirac, N. Adimi, B. Blank, C. Borcea, B.A. Brown, I. Companis, F. Delalee, C.E. Demonchy, F. de Oliveira Santos, J. Giovinazzo, S. Grévy, L.V. Grigorenko, T. Kurtukian-Nieto, S. Leblanc, J.-L. Pedroza, L. Perrot, J. Pibernat, L. Serani, P.C. Srivastava, J.-C. Thomas, Direct observation of two protons in the decay of ^{54}Zn, Phys. Rev. Lett. 107 (2011) 102502.

[42] P. Moller, J. Nix, W. Myers, W. Swiatecki, Nuclear ground-state masses and deformations, At. Data Nucl. Data Tables 59 (1995) 185–381.

[43] R.A. Kryger, A. Azhari, M. Hellström, J.H. Kelley, T. Kubo, R. Pfaff, E. Ramakrishnan, B.M. Sherrill, M. Thoennessen, S. Yokoyama, R.J. Charity, J. Dempsey, A. Kirov, N. Robertson, D.G. Sarantites, L.G. Sobotka, J.A. Winger, Two-proton emission from the ground state of ^{12}O, Phys. Rev. Lett. 74 (1995) 860–863.

[44] F.C. Barker, Width of the ^{12}O ground state, Phys. Rev. C 59 (1999) 535–538.

[45] G. Audi, F.G. Kondev, M. Wang, W.J. Huang, S. Naimi, The NUBASE2016 evaluation of nuclear properties, Chin. Phys. C 41 (2017) 30001.